Ceramics International 43 (2017) 4272–4279

Contents lists available at ScienceDirect

Ceramics International

journal homepage: www.elsevier.com/locate/ceramint

Influence of different chemical treatments on the surface of Al_2O_3/ZrO_2 nanocomposites during biomimetic coating

Kátia Helena dos Santos[a], Julieta Adriana Ferreira[a,*], Denise Osiro[a], Gelson José Andrade da Conceição[a], Rubens Bernardes Filho[b], Luiz Alberto Colnago[b], Eliria Maria de Jesus Agnolon Pallone[a]

[a] Department of Biosystems Engineering, University of Sao Paulo, USP, Av. Duque de Caxias Norte, 225, Pirassununga, SP CEP 13635-900, Brazil
[b] Brazilian Agricultural Research Corporation, EMBRAPA Instrumentation, Rua Quinze de Novembro, 1500/1501, São Carlos, SP CEP13561-206, Brazil

ARTICLE INFO

Keywords:
Nanocomposites
Calcium phosphate
Chemical treatments
Biomimetic coating
Alumina-zirconia

ABSTRACT

The objective of this study is to evaluate the influence of different chemical surface treatments (H_3PO_4, HNO_3, and NaOH) in the formation of calcium phosphate phases on the surface of Al_2O_3/ZrO_2 (5 vol%) nanocomposite. For this purpose, Al_2O_3/ZrO_2 samples were shaped, calcined at 400 °C, sintered at 1500 °C, subjected to different chemical treatments, and biomimetically coated from 14 to 21 days. Surface characterization was performed by scanning electron microscopy, atomic force microscopy, confocal microscopy, X-ray diffraction, and infrared spectroscopy. It was observed that the preliminary chemical treatment favored the formation of particular calcium phosphate phases of interest, such as α-TCP (alpha-tricalcium phosphate), β-TCP (beta-tricalcium phosphate), and HA (hydroxyapatite). The differences among the percentages of the phases formed affected the homogeneity of calcium phosphate distribution within the nanocomposites as well as the roughness of the formed layer, effectively contributing to adhesion, proliferation, and desired cell biofixation on bone implant.

1. Introduction

Numerous advances have been recently made in the development of novel synthetic materials for the improvement of bone structural recoveries, grafts, implants, and orthopedic surgery, among others [1]. The materials commonly used for these purposes are called biomaterials and must meet physical and biological properties compatible with host living tissue in order to stimulate an appropriate response [2].

These characteristics are specially found in ceramic based calcium phosphates which resemble the mineral phase of bones. However, an important detrimental aspect of these ceramic materials is their low mechanical strength and fracture toughness [3]. To increase their mechanical resistance, it is necessary to combine them with other materials resulting in ceramic matrix nanocomposites.

The inclusion of nanometric ZrO_2 in Al_2O_3 matrix results in significant improvements in microstructural homogeneity as well as increased mechanical properties when compared to inclusion-free Al_2O_3 [4]. Under physiological conditions, Al_2O_3/ZrO_2 nanocomposite is virtually inert, leading to little or no response from surrounding tissues, so it remains essentially unchanged [5].

The bioinert nature of these nanocomposites has stimulated the development of new techniques to make the biological performance of these ceramics more suitable [6], among which biomimetic coating stands out. It consists of the immersion of a substrate into a fluid with ions concentration equal to blood plasma, allowing the formation of a bioactive coating on the surface of the substrate [7].

Since its first occurrence, biomimetic coating has undergone remarkable changes to accelerate the deposition process and to change the crystallinity of the coating. In 2002, Barrere *et al.*[8] evaluated changes in the concentration of SBF (Synthetic Body Fluid) solution originally of 1.5SBF to more concentrated 5.0SBF, aiming at coating a metallic substrate. The authors found that the Ca/P coating formed on the surface of the substrate was significantly thicker in the samples subjected to the more concentrated solution compared to those coated with the original solution (i.e., 1.5SBF).

The interaction between the formed phosphate layer and the nanocomposite surface may be improved by means of preliminary treatments (i.e., prior to the biomimetic coating). In this sense, carrying out a preliminary surface activation process (e.g., chemical treatments with acidic or alkaline solutions) relies upon the fact that it provides suitable interfacial attachment between the bioinert material

* Corresponding author.
E-mail address: julieta.ferreira@usp.br (J.A. Ferreira).

http://dx.doi.org/10.1016/j.ceramint.2016.12.069
Received 28 September 2016; Received in revised form 2 December 2016; Accepted 12 December 2016
Available online 19 December 2016

and the formed bioactive layer [9].

The adhesion and morphology of the bioactive layer formed on the substrate depend on the material's surface properties [9]. For this reason, surface roughness is an important property, making confocal microscopy an important tool to characterize biomaterials [10]. The use of this technique allows the quantification of different roughness parameters, being average roughness (Ra) the most widely used parameter in the study of surface roughness of materials [10].

Bioactive ceramic surfaces are prone to apatite crystal nucleation and growth. Accordingly, several methods have been used to characterize the apatite layer formed on the surfaces of biomaterials, including Fourier transform infrared (FTIR) spectroscopy and X-ray diffraction (XRD) [11–13].

Different factors (e.g., size and suitable morphology) determine the successful implementation of an implant as well as influence host tissue response. Cellular activity may also be affected by particle shape; spherical particles being preferred over sharp particles because injuries in the cell cytoplasm are prevented. According to studies carried out by Uchida et al. [14], apatite-forming ability on a surface may be influenced by the type of solution in which the surface was treated. In studies performed by Wu et al. [15] on precipitation or crystallization processes of a solid phase from solution (e.g., SBF), competition between crystal nucleation and growth phenomena was evidenced. The competition between these two phenomena, in different saturation stages, may determine the size and the morphology of the future crystal.

In this context, this study aimed to evaluate the influence of different chemical surface treatments (H_3PO_4, HNO_3, and NaOH) in the formation of calcium phosphate phases on the surfaces of Al_2O_3/ZrO_2 (5 vol%) nanocomposites submitted to different biomimetic coating times.

2. Experimental procedure

To carry out this study, we used as raw materials 99.995% commercial Al_2O_3 powder (AKP-53, Sumitomo Chemical Co., Japan) with an average particle size of 0.2 μm, and 99.900% monoclinic ZrO_2 nanoparticles (Nanostructured Materials Inc.) with an average size of 50 nm. Powder mixing (95 vol% Al_2O_3 and 5 vol% ZrO_2) and specimen conformation protocols were in accordance with Chinelatto et al., 2014 [16]. The specimens were calcined at 400 °C/1 h and sintered at 1500 °C/2 h [17]. The sintered samples were characterized for apparent density following the Archimedes principle and by X-ray diffraction (XRD Rigaku, Miniflex 600). Microstructural analyses by scanning electron microscopy (Phillips XL30 FEG-SEM) were performed on the polished and thermally etched sintered surfaces at 1450 °C/10 min.

Hardness was measured by using the indentation technique (Buehler, model Micromet 5104) with a conventional diamond pyramid indenter, applying a load of 0.5 kgf [18]. The measurement of the fracture toughness as a function of the crack length was conducted using the indentation technique applying a load of 2Kgf and time of 60 s. From the recorded crack length and applied load, the mode-I stress-intensity factor was determined according to ASTM standard C 1421-99 [19].

Once sintered, the samples were immersed in either water or in H_3PO_4 5 M, HNO_3 5 M or NaOH 15 M solution, at 90 °C for 4 days, under reflux and thermostatic bath. After the chemical treatment, the samples were washed in distilled water and dried in a desiccator at room temperature [14]. The surfaces were characterized by confocal microscopy (Olympus, Lext-OLS 4100) and Fourier Transform Infrared spectroscopy (FTIR Spectrometer, Vertex 70 Bruker). Average roughness (Ra) was calculated from four points imaged by confocal microscopy for 6 different samples, totaling 24 Ra values for each treatment.

After the chemical surface treatment, the samples were coated by biomimetic method according to the procedure proposed by Barrere et al. [8], using a SBF (Synthetic Body Fluid) solution with concentration five times greater than the original SBF solution proposed by Abe et al. [7]. After incubation for 14 and 21 days at 36.5 °C under constant stirring (60 rpm), the coated samples were washed and dried in a desiccator at room temperature. The surfaces were characterized by atomic force microscopy (AFM NanoSurf Flex), FTIR spectroscopy, and XRD. The XRD patterns and the FTIR absorbance spectra were mathematically treated, their baselines were corrected, and their second derivatives were calculated. The Gaussian function was used to fit all the deconvoluted curves. The correlations between the different calcium phosphate phases observed by XRD and FTIR were performed using the Pearson's Correlation Coefficient (r). Statistical significance was considered at $p < 0.05$.

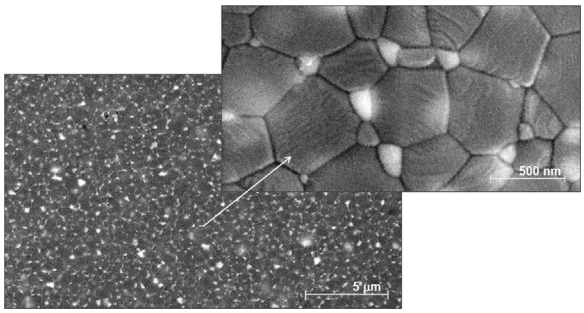

Fig. 1. SEM micrographs of the surface of the Al_2O_3/ ZrO_2 nanocomposite.

3. Results and discussion

3.1. Microstructural characterization of the Al_2O_3/5 vol%ZrO_2 nanocomposites

Fig. 1 shows SEM micrographs of the polished, thermally attacked surface of the Al_2O_3/ZrO_2 nanocomposite sintered at 1500 °C for 2 h prior to any chemical treatment. The ZrO_2 inclusions (brighter regions) were uniformly spread within the Al_2O_3 matrix, suggesting that the processing protocol effectively prevented the formation of fine particle clusters in the matrix. We also observed that the ZrO_2 inclusions were located at the grain boundaries, including triple points, resulting in an intergranular-type nanocomposite, as detailed in the figure. The ZrO_2 inclusions at these positions favored the pinning (anchoring) of the Al_2O_3 grain boundaries, thereby inhibiting the grain growth of the matrix [20].

The Al_2O_3/ZrO_2 nanocomposite presented an apparent density of 97.20 ± 0.92%, a hardnessof 15.40 ± 0.22 GPa and a fracture toughness of 3.72 ± 0.43 MPa $m^{1/2}$. The hardness and the fracture toughness of the cortical bone are reported be in the range of 9.6–17.4 GPa and 2–12 MPa $m^{1/2}$ [21] respectively, suggesting that these nanocomposites are potential replacements for cortical bones.

3.2. Surface characterization of the Al_2O_3/5 vol%ZrO_2 nanocomposites after the chemical treatments

The average roughness (Ra) values of the chemically treated and untreated surfaces of the Al_2O_3/ZrO_2 nanocomposites were as follows: treated with NaOH: 0.054 ± 0.010 μm; treated with HNO_3: 0.045 ± 0.003 μm; and treated with H_3PO_4: 0.059 ± 0.008 μm. The Ra of the untreated sample was 0.045 ± 0.002 μm. Overall, the different chemical treatments of the nanocomposites lead to different surface roughness. These differences may act as starter sites by triggering nucleation and/or crystal growth. It is worth mentioning that this characteristic is highly desirable as it can ensure a more homogeneous and effective adhesion of a biomimetic coating [14].

Fig. 2 shows the second derivatives of the FTIR spectra from 425 to 4000 cm^{-1} of the Al_2O_3/ZrO_2 nanocomposites submitted to different

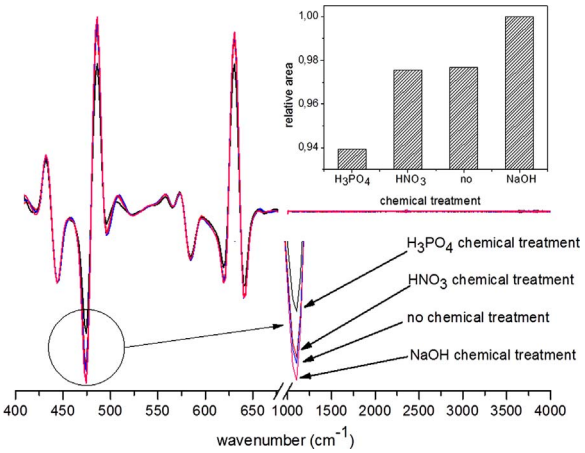

Fig. 2. Second derivative of the FTIR spectra of Al_2O_3/ZrO_2 nanocomposites either untreated or chemically treated with H_3PO_4, HNO_3 or NaOH. The insert presents the relative areas of the FTIR spectra within the range of 425–4000 cm^{-1} for all studied conditions.

chemical treatment conditions in addition to the chemically untreated sample. The areas related to the spectra of each specific chemical treatment are also shown.

The absorption bands above the spectral region of 1000 cm^{-1} were not observed for any of the chemical treatment conditions of the Al_2O_3/ZrO_2 nanocomposites. The absence of the absorption bands in the spectral regions around 3656 cm^{-1} (stretching vibration of OH physically adsorbed to Al^{+3}), at 3447 cm^{-1} (stretching vibrations of OH groups), around 1638 cm^{-1} (bending vibrations of H_2O molecules), around 1070 cm^{-1} (bending vibration of Al–OH groups) and at ~1764/~1634/~1385 cm^{-1} (bending vibration of Zr–OH groups) may be explained by the removal of surface water from the Al_2O_3/ZrO_2 nanocomposites, resulting in a fully anhydrous crystalline structure [22,23]. The peaks at 640 and 580 cm^{-1} observed may be attributed to Al–O bending vibrations, whereas the peaks at 621, 475 and 445 cm^{-1} observed in the same spectra may be assigned to Zr–O.

All the FTIR spectra were expected to present the same intensity and/or relative area of the characteristic absorption bands of the Al_2O_3/ZrO_2 nanocomposites. However, the relative areas of these absorption bands (shown in the insert of Fig. 2) are believed to be dependent on chemical treatment. In general, the relative area of the FTIR spectrum obtained for the nanocomposite chemically treated with H_3PO_4 was smaller than that obtained for the nanocomposite chemically treated with NaOH. This behavior is clearly shown by the intensity differences presented by the absorption bands at 475 cm^{-1} assigned to the vibration of the Zr–O group [11] of the Al_2O_3/ZrO_2 nanocomposite (Fig. 2).

Average roughness is commonly associated with the presence of protrusions on the surface of a nanocomposite, directly affecting its wettability [24]. Brandão et al. [25] reported that the hydrophilic or hydrophobic behavior of a surface is related to its surface energy: higher energy and greater wettability. According to Gennes, 1985 [26], surfaces of hard-type solids (which have covalent, metallic or ionic bonds) have a hydrophilic character and, therefore, present high wettability.

As a consequence, the smaller relative area observed in the FTIR spectrum of the Al_2O_3/ZrO_2 nanocomposite chemically treated with H_3PO_4, as well as the larger Ra value, suggests the presence of a more hydrophilic surface than the nanocomposite chemically treated with NaOH (larger relative area), for instance. This can be due to wettability associated with improved affinity for adsorption [25]. The hydrophilic character of the Al_2O_3/ZrO_2 nanocomposite surface may contribute effectively to the deposition of calcium phosphate on the nanocomposite surfaces.

Another interesting feature observed in the FTIR spectra of the nanocomposites is the absence of the absorption band related to the stretching and bending vibrations of the Me–OH groups [27] in the region between 2300 and 2400 cm^{-1}. The absence of the vibrations of the Me–OH group on the surface of the nanocomposite studied suggests that the different chemical treatments neither formed Zr–OH nor Al–OH groups on the surfaces.

3.3. Characterization of the surface of Al_2O_3/5 vol%ZrO_2 nanocomposites coated by the biomimetic method

Fig. 3 shows the FTIR spectra for absorbance and second derivative, at wavelengths ranging from 970 to 1200 cm^{-1}, of the surfaces of Al_2O_3/ZrO_2 nanocomposites submitted to different chemical treatments (untreated or treated with H_3PO_4, HNO_3 or NaOH) after 14 and 21 days of biomimetic coating. The shifts of the deconvoluted curves under the spectra were analyzed according to other authors [11,12]. The intensities of the FTIR absorbance spectra were normalized by the intensity of the band between 400 and 500 cm^{-1}, which in

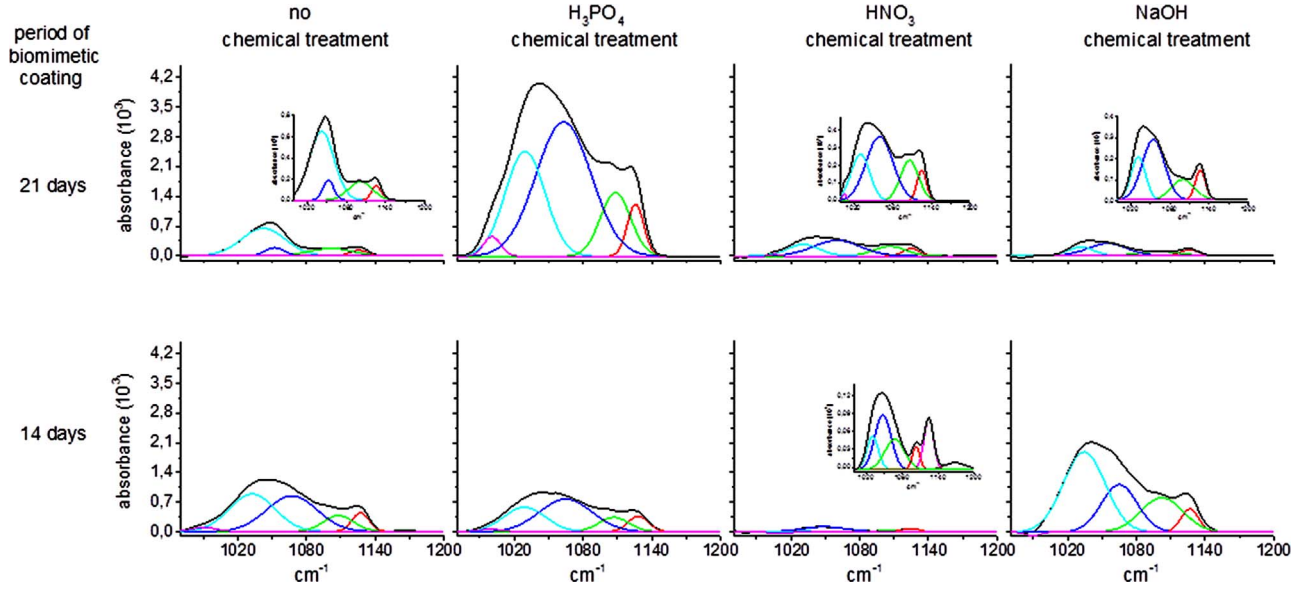

Fig. 3. FTIR absorption spectra of the surfaces of Al_2O_3/ZrO_2 nanocomposites submitted to different chemical treatments (untreated or treated with H_3PO_4, HNO_3 or NaOH) before and 14 and 21 days after the biomimetic coating. The insert presents the intensities of the absorbance spectra within the range of 980–1200 cm^{-1} for some studied conditions.

Table 1
Areas (%) under the deconvoluted curves of the FTIR absorbance spectra related to the calcium phosphate formed on the surfaces of Al_2O_3/ZrO_2 nanocomposites submitted to different chemical treatments (untreated or treated with H_3PO_4, HNO_3 or NaOH) after 14 and 21 days of biomimetic coating.

Chemical surface treatment													
Untreated				H_3PO_4				HNO_3				NaOH	
Period of biomimetic coating (days)													
14		21		14		21		14		21		14		21	
Area (%)	Band (cm^{-1})	Area (%)	Band (cm^{-1})	Area (%)	Band (cm^{-1})	Area (%)	Band (cm^{-1})	Area (%)	Band (cm^{-1})	Area (%)	Band (cm^{-1})	Area (%)	Band (cm^{-1})	Area (%)	Band (cm^{-1})
7.26	1127	5.54	1126	8.92	1128	5.87	1126	17.41	1125	7.99	1125	5.92	1126	10.94	1127
10.95	1108	17.65	1101	12.35	1107	13.05	1108	6.61	1104	20.20	1106	20.93	1100	16.95	1102
40.85	1067	8.67	1052	48.21	1065	50.42	1063	69.98	1049	47.05	1060	24.55	1056	49.33	1065
38.68	1033	68.14	1042	28.76	1029	28.33	1030	6.00	1031	23.99	1031	48.60	1032	22.78	1035
2.26	991	0.00	991	1.76	999	2.33	1003	0.00	1006	0.77	1006	0.00	990	0.00	990

turn was attributed to vibrations of the Al–O group. The intensities of the second derivative FTIR spectra were normalized by the peak at 445 cm^{-1} attributed to vibrations of the groups as well as to Zr–O.

Table 1 shows the percent areas under the deconvoluted FTIR curves (absorbance spectra) related to the calcium phosphate formed on the surface of the Al_2O_3/ZrO_2 nanocomposite by different chemical treatments (untreated or treated with H_3PO_4, HNO_3 or NaOH), 14 and 21 days after the biomimetic coating. Absorption bands typical of phosphate groups were observed 14 and 21 days after the biomimetic coating in the spectral region between 970 and 1200 cm^{-1}. Absorption bands at 990–991 cm^{-1} are attributed to the symmetric P–O stretching from the PO_4^{3-} group. Absorption bands between 1029 and 1035 cm^{-1} are attributed to the triply degenerated asymmetric P–O stretching mode from the PO_4^{3-} group. Absorption bands from 1049 to 1065 cm^{-1} are assigned to the triply degenerated asymmetric P-O stretching mode from the PO_4^{3-} group and the α-TCP phase. Absorption bands in the region between 1100 and 1108 cm^{-1} are assigned to the HPO_4^{2-} groups from the nonstoichiometric hydroxyapatite (HA) (presence of crystal imperfections and HPO_4^{2-} groups in nonstoichiometric HA). Finally, absorption bands observed in the region between 1125 and 1128 cm^{-1} are also assigned to the HPO_4^{2-} from the nonstoichiometric HA as well as from the β-TCP phase (presence of crystal imperfections and HPO_4^{2-} groups in nonstoichiometric HA and β-TCP). The positions of the peaks observed in the second derivative spectra (cm^{-1}), within the phosphate regions (970–1200 cm^{-1}), as well as their attributions in accordance to the literature, are summarized in Table 2[11,12,28].

Overall, after 21 days of incubation, the percentages of the areas under the absorption bands in the regions between 1029 and 1035 cm^{-1} as well as between 1100 and 1008 cm^{-1} increased in the chemically untreated Al_2O_3/ZrO_2 nanocomposites and in those treated with H_3PO_4 and HNO_3. During the same incubation period, the percentages of the areas under the absorption bands from 1049 to 1065 cm^{-1} decreased in the chemically untreated Al_2O_3/ZrO_2 nanocomposites and in those treated with H_3PO_4 and HNO_3.

The areas under the absorption band attributed to the formation of the α-TCP phase simultaneously decreased with increasing area under the absorption band attributed to the formation of the HA phase. This can suggest that the α-TCP phase may be contributing to the formation of the HA phase, which is more stable after 21 days of incubation.

On the other hand, there was a decrease in the percentage of the areas under the absorption bands from 1029 to 1035 cm^{-1} and from 1100 to 1008 cm^{-1} in the Al_2O_3/ZrO_2 nanocomposites chemically treated with NaOH, after 21 days of incubation. For the same conditions, there was an increase in the percentage of the area under the absorption band in the region between 1049 and 1065 cm^{-1}. It is worth emphasizing that the surfaces of the nanocomposites treated with NaOH presented coating failures after 21 days of incubation. This finding may be a result of the decreased HA content as well as the increased amount of α-TCP formed on the nanocomposite surfaces during the longest incubation time.

Fig. 4 presents the XRD pattern, from 31.0 to 34.0°, of the calcium phosphate formed on the surface of the Al_2O_3/ZrO_2 nanocomposites submitted to different chemical treatments (untreated or treated with H_3PO_4, HNO_3 or NaOH), 14 and 21 days after the biomimetic coating. The shifts of the deconvoluted curves under the diffractograms relied upon the standard Miller indices (*hkl*) for each calcium phosphate layer, in accordance with the database (JCPDS) [29].

The mathematical fitting of the XRD pattern using a Gaussian function allows the attainment of deconvoluted analytical curves and, as a result, it is possible to identify and quantify the different calcium phosphate phases formed on the surfaces of the Al_2O_3/ZrO_2 nanocomposites in any incubation period.

Consequently, the deconvolution of the curves under the XRD patterns (Fig. 3) revealed the formation of three distinct calcium phosphate phases on the nanocomposite surfaces. Thus, it was possible to distinguish the growth of crystals of the α-tricalcium phosphate (α-

Table 2
Peak positions (cm^{-1}) observed in the FTIR spectra of the second derivative in the regions typical of phosphates as well as their attributions according to data published in the literature [11,12,28].

Peak Positions (cm^{-1})	Assignments
990–991 (w)	PO_4^{3-}, symmetric stretching mode of the P–O bonds of the phosphate group
1029–1035 (sh)	v_{3c}, PO_4^{3-}, Triply degenerated asymmetric stretching mode of the P–O bond of the phosphate group, occurring in stoichiometric apatites
1049–1065 (s)	v_{3b}, PO_4^{3-}, Triply degenerated asymmetric stretching mode of the P–O bond of the phosphate group and stretching mode of αTCP
~1081 (s)	v_{3a}, PO_4^{3-}, Triply the phosphate group
1100–1108	Due to the presence the crystal imperfections and HPO_4^{2-} groups in nonstoichiometric HA
1125–1128	Due to the presence the crystal imperfections and HPO_4^{2-} groups in nonstoichiometric HA and stretching mode of βTCP

TCP) phase in the (511) plane (09-348 JCPDS), of the β-tricalcium phosphate (β-TCP) phase in the (128) plane (09–169 JCPDS), and also of the hydroxyapatite (HA) phase in the (211)/(112) planes (09-432 and 73-1731 JCPDS) [29]. It is noteworthy that all of the three calcium phosphate layers were observed in all incubation periods regardless of the chemical treatment received by the nanocomposite.

Table 3 shows the percentages of the different calcium phosphate phases (α-TCP, β-TCP, and HA) formed on the surface of the Al_2O_3/ZrO_2 nanocomposites submitted to different chemical treatments (untreated or treated with H_3PO_4, HNO_3 or NaOH) after 14 and 21 days of biomimetic coating. After incubation for 14 days, there was a greater amount of αTCP phase in the chemically untreated Al_2O_3/ZrO_2 nanocomposites (32.82%). Contrastingly, the nanocomposites chemically treated with NaOH exhibited lower formation of this phase (10.40%) in the same biomimetic coating period. After 21 days of incubation, however, the α-TCP phase percentage decreased in the chemically untreated nanocomposites (51.50% reduction) and in those chemically treated with H_3PO_4 (49.730% reduction) and HNO_3 (reduction of 69.20%). On the surfaces of the nanocomposites that were chemically treated with NaOH, the αTCP phase content increased by 137.90%.

After 21 days of incubation, the formation of β-TCP phase on the surface of the Al_2O_3/ZrO_2 nanocomposites significantly increased in the sample chemically treated with H_3PO_4 (145.50% increase). It was also increased, though less pronounced, in the chemically untreated nanocomposites (29.20 increase %). In the other nanocomposites, however, the increased formation of the β-TCP phase throughout the biomimetic coating was barely noticeable: 2.60% for the nanocomposite treated with HNO_3 and 1.20% for that treated with NaOH.

The higher percentage of β-TCP phase observed on the surfaces of all Al_2O_3/ZrO_2 nanocomposites, regardless of the chemical surface treatment or the coating period, is due to the greater thermodynamic stability of this phase when compared to the α-TCP phase. The allotropic forms α and β-TCP may also be osteoconductive, but the α-TCP phase has greater bioactivity features due to its structural arrangement. Due to the bioabsorbable nature of the TCPs, biological calcifications originating from this phase do not occur. However, the formation of the β-TCP phase is favored when the Mg/Ca molar ratio in solution is greater than 0.05, leading to the formation of the beta-magnesium tricalcium phosphate (β-Mg-TCP) phase [30–34]. Hence, the increased formation of β-TCP phase on the nanocomposite surfaces throughout the different incubation periods studied are explained by the high Mg/Ca ratio (0.83) contained in the SBF used.

Overall, after 21 days of incubation, the HA phase formed on the nanocomposite surfaces varied from 51% to 74%. Except for the nanocomposites chemically treated with NaOH, increased HA formation was observed throughout the incubation period. It is worth mentioning that such increase was higher in the chemically untreated nanocomposites (23.30% increase). The increased HA formation, though less remarkable, was also noticed in the nanocomposites submitted to chemical treatment with HNO_3 (10.20% increase) and H_3PO_4 (increase of 2.70%). For those chemically treated with NaOH, on the other hand, HA formation decreased by 22.70%, 21 days after the coating.

Generally, the consumption of the α-TCP phase (observed in the FTIR absorbance bands) strongly correlated with the formation of the HA phase (observed in the XRD patterns), as evidenced by the Pearson correlation coefficient ($r_{\mathrm{FTIR}\alpha TCP\ /\ \mathrm{XRD}HA}$=0.78). Another interesting correlation was observed between the decreased αTCP content (observed in the XRD patterns) and the increased βTCP formation (observed in the FTIR absorbance bands) after 21 days of incubation, also being indicated by the Pearson coefficient correlation ($r_{\mathrm{FTIR}\alpha TCP\ /\ \mathrm{XRD}\beta TCP}$ =0.87).

As previously mentioned in this text, the crystal growth of the

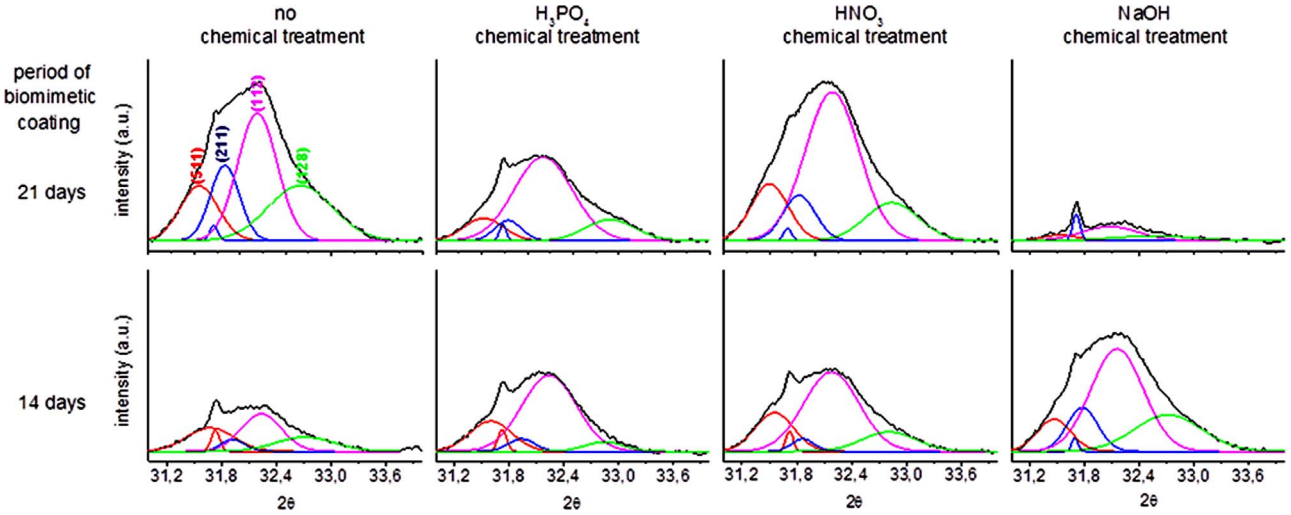

Fig. 4. XRD patterns, from 31.0 to 34.0°, of the calcium phosphate formed on the surfaces of Al_2O_3/ZrO_2 nanocomposites submitted to different chemical treatments (untreated or treated with H_3PO_4, HNO_3 or NaOH) after 14 and 21 days of biomimetic coating. The insert presents the intensities of the deconvoluted curves and XRD patterns for NaOH chemical treatment after 21 days of biomimetic coating. The deconvoluted curves were based on the standard Miller indices (*hkl*) for the calcium phosphates, according to the JCPDS [29].

Table 3
Percentages of the different calcium phosphate phases formed on the surfaces of Al_2O_3/ZrO_2 nanocomposites submitted to different chemical treatments (untreated or treated with H_3PO_4, HNO_3 or NaOH) after 14 and 21 days of biomimetic coating. The percentages were calculated from the standard reflection indices *hkl* for the calcium phosphate family, according to the JCPDS [29].

Chemical surface treatment		**Untreated**		**H_3PO_4**		**HNO_3**		**NaOH**	
Period of biomimetic coating (days)		**14**	**21**	**14**	**21**	**14**	**21**	**14**	**21**
[a]***hkl* reflections**	(511)	32.82	15.91	23.19	11.75	22.14	15.31	10.40	24.74
	(211)	7.24	17.81	5.28	8.70	3.73	11.43	13.88	49.92
	(112)	38.67	38.80	65.81	65.53	59.78	58.53	52.05	1.39
	(128)	21.27	27.47	5.71	14.02	14.35	14.73	23.66	23.94

[a] Standard reflection indices Miller according to the JCPDS.

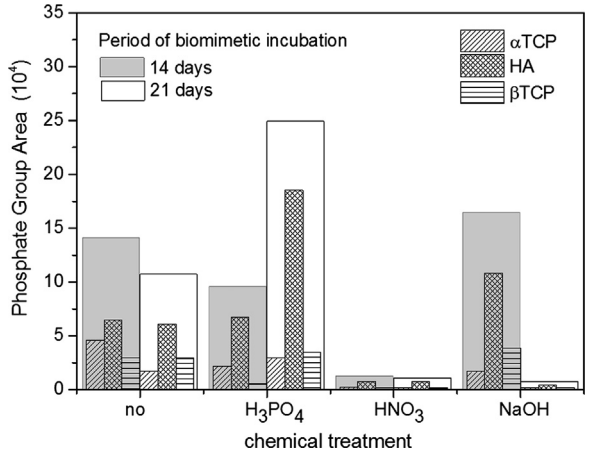

Fig. 5. Values of total area – calculated from the FTIR absorbance spectra – and percentages of the calcium phosphate phases – calculated by XRD – for the nanocomposites submitted to different chemical treatments, after 14 and 21 days of biomimetic coating.

αTCP, βTCP and HA phases on the surface depended on the different chemical treatments. Fig. 5 shows the areas under the FTIR absorbance spectra of the calcium phosphates from 980 to 1150 cm^{-1}, as well as the calcium phosphate phase percentages – measured by XRD – formed on the surfaces of the nanocomposites (untreated or treated with H_3PO_4, HNO_3, and NaOH) after 14 and 21 days of coating. From these results, it is possible to determine the amount of calcium phosphates formed on the surfaces, as well as estimate the minimum time required for coating in a particular condition. For instance, after 21 days of incubation, the surfaces of the nanocomposites treated with NaOH showed some coating failures. This behavior revealed the lower HA content on the surfaces (96.30% decrease), suggesting that the 14-d incubation period is appropriate for these nanocomposites. Another interesting factor is the possibility of choosing the percentages of calcium phosphate phases formed. For example, if a higher amount of TCP is needed, 14 days of incubation of the chemically untreated nanocomposites would provide 54.10% of TCP and 45.90% of HA. On the other hand, if the HA phase is required to be prevalent, this could be achieved after 21 days of coating the nanocomposites chemically treated with H_3PO_4 (74.20% of HA and 25.80% of TCP). It is also noteworthy that the nanocomposites chemically treated with H_3PO_4 showed higher (51.90% increase) calcium phosphate contents 21 days after coating.

Fig. 6 shows AFM images of the surface of the Al_2O_3/ZrO_2 nanocomposites with different chemical treatments (untreated or treated with H_3PO_4, HNO_3 or NaOH) after 21 days of biomimetic coating. The Ra values after 21 days of biomimetic coating were as follows: treated with NaOH: 0.753 ± 0.103 μm; treated with HNO_3: 2.658 ± 0.2108 μm; and treated with H_3PO_4: 3.346 ± 0.143 μm. The Ra of the untreated coated sample was 2.305 ± 0.037 μm. In general, the homogeneity of the calcium phosphate distribution within the layer formed on the Al_2O_3/ZrO_2 nanocomposite surface was different for each chemical treatment to which the nanocomposites were submitted. We also noticed that these calcium phosphate globules had different sizes depending on the chemical treatment. Among the tested conditions, the globules over the nanocomposites chemically treated with H_3PO_4 were smaller than those formed by other chemical treatments. It appears that the smaller globules provided the calcium phosphate layer with a rougher appearance on the surface of the Al_2O_3/ZrO_2 nanocomposites. This behavior may be associated with increased roughness (greater Ra value, 3.346 ± 0.143 μm) and to higher hydrophilic character of the surfaces of the Al_2O_3/ZrO_2 nanocomposites chemically treated with H_3PO_4, playing a role in the way in which calcium phosphate is deposited onto the nanocomposite surface [35,36].

The relationship between the distribution of calcium phosphate globule over the nanocomposite surfaces and the chemical treatments to which the nanocomposite was submitted is quite attractive because the interaction among cells, tissues and implants can be affected by the surface area of the implant. It is expected that the greater the implant surface roughness, the greater the number of cell sites available for binding, thereby facilitating tissue growth on such a surface. On the other hand, the roughness level must be controlled due to the need for anchoring points on the implant surface in order to trigger cell proliferation, thus ensuring cell biofixation. If the surface roughness happens to be much smaller than the cell size, however, attachment sites may be absent, thus affecting the type of cellular proliferation. Epithelial, macrophage and osteoblast cells, to mention a few, adhere more easily to rough surfaces, whereas fibroblast cells accumulate in smoother regions [37–39]. Thus, the chemical surface treatments that the Al_2O_3/ZrO_2 nanocomposites undergo prior to the biomimetic coating are believed to effectively contribute to the adhesion, proliferation and biofixation of the desired cell type on bone implants.

4. Conclusions

In summary, the preliminary chemical surface treatments of the systems studied can be an important step and plays a role in the surface roughness of the nanocomposites. Consequently, differences in surface roughness may act as nucleation and crystal growth sites, contributing to the effective adhesion of calcium phosphate on the surfaces of the Al_2O_3/ZrO_2 nanocomposites. Additionally, it was observed that the different chemical treatments influenced the amount of calcium phosphate formed on the nanocomposite surfaces as well as the minimum incubation time, favoring the formation of a particular calcium phosphate phase. For the different amounts of the phases formed on the nanocomposite surfaces, calcium phosphate globules distribution and layer roughness were homogeneous, potentially contributing, in an effective way, to the desired adhesion, proliferation, and cell biofixation on bone implants.

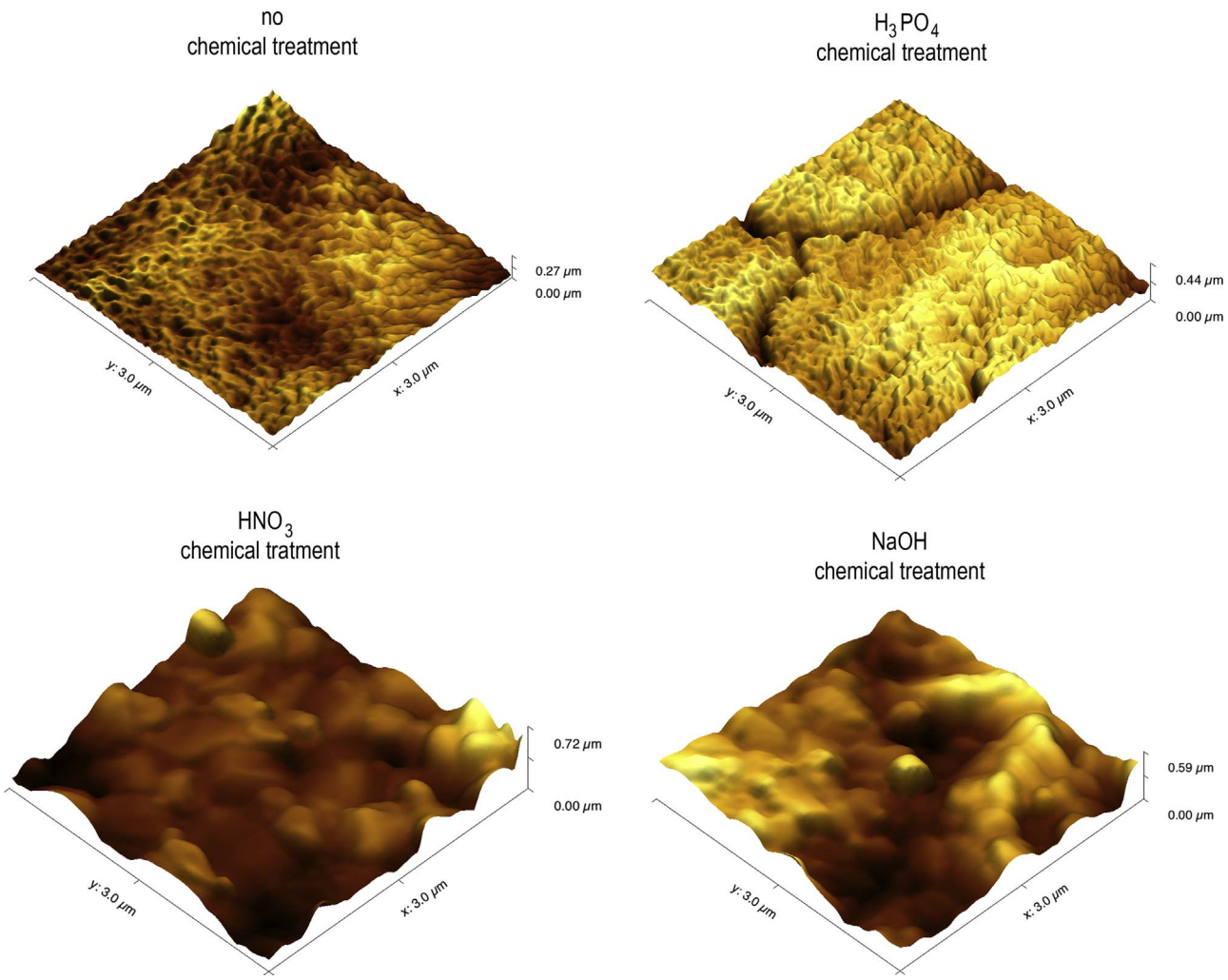

Fig. 6. AFM images of the surfaces of Al_2O_3/ZrO_2 nanocomposites submitted to different chemical treatments (untreated or treated with H_3PO_4, HNO_3 or NaOH) after 21 days of biomimetic coating.

Acknowledgments

The authors gratefully acknowledge the financial support of the Brazilian Research Funding Agency FAPESP (São Paulo Research Foundation, process no 2014/11100-9), CNPq (National Council for Scientific and Technological Development, Research Productivity Grant process no 306114/2013-5) and CAPES (Coordination for the Improvement of Higher Education Personnel) (process no. 23038.009604/2013-12).

References

[1] B.D.Ratner, A.S.Hoffman, F.J.Schoen, J.E.Lemons, Biomaterials science an introduction to materials in medicine, 3rd edition, 2013.
[2] F.M. Cheng, X. Liu, Advancing biomaterials of human origin for tissue engineering, Prog. Polym. Sci. 53 (2016) 86–168.
[3] X. Zheng, F. Zhao, J. Zhang, Mechanical properties and fracture behaviour of multilayer alumina composites, J. Wuhan. Univ. Technol. 30 (5) (2015) 965–967.
[4] S. Siqueira, M.H. Fernandes, N. Neves, M.M. Almeida, Development and characterization of zirconia-alumina composites for orthopedic implants, Ceram. Int. 43 (1) (2017) 693–703.
[5] C.L. Ojaimi, A.S.A. Chinelatto, A.L. Chinelatto, E.M.J.A. Pallone, R.E.P. Salem, Microstructural evolution of alumina-zirconia nanocomposites, Mater. Sci. Forum 805 (2015) 621–626.
[6] J. Li, G.W. Hastings, Oxide Bioceramics: inert ceramic materials in medicine and dentistry, Handb. Biomater. Propert. (2016), 339–352.
[7] Y. Abe, T. Kokubo, T. Yamamuro, Apatite coating on ceramics, metals and polymers utilizing a biological process, J. Mater. Sci. Mater. Med. l (1990) 233–238.
[8] F. Barrere, C.A. Van Blitterswijk, K. Groot, P. Layrolle, Influence of ionic strength and carbonate on the Ca-P coating formation from SBF×5 solution, Biomaterials 23 (29) (2002) 1921–1930.
[9] M.G. Faga, A. Vallée, A. Bellosi, M. Mazzocchi, N.N. Thinh, G. Martra, S. Coluccia, Chemical treatment on alumina-zirconia composites inducing apatite formation with maintained mechanical properties, J. Eur. Ceram. Soc. 32 (2012) 2113–2120.
[10] R.S. Austin, C.L. Giusca, G. Macaulay, R. Moazzez, D.W. Bartlett, Confocal laser scanning microscopy and area-scale analysis used to quantify enamel surface textural changes from citric acid demineralization and salivary remineralization in vitro, Dent. Mater. 32 (2016) 278–284.
[11] L. Berzina-Cimdina, N. Borodajenko, Research of calcium phosphates using fourier transform infrared spectroscopy, Infrared Spectroscopy. J. Mater. Sci. Eng. Technol., Prof. Theophanides Theophile (Ed.) (2012) 123–149.
[12] G. Piga, D. Gonçalves, T.J.U. Thompson, A. Brunetti, A. Malgosa, S. Enzo, Understanding the crystallinity indices behavior of burned bones and teeth by ATR-IR and XRD in the presence of bioapatite mixed with other phosphate and carbonate phases, Int. J. Spectrosc. (2016) 1–9.
[13] H. Gollwitzer, X. Yang, L. Spevak, L. Lukashova, A. Nocon, K. Fields, N. Pleshko, H.W. Courtland, M.P. Bostrom, A.L. Boskey, Fourier transform infrared spectroscopic imaging of fracture healing in the normal mouse, Int. J. Spectrosc. (2016) 1–13.
[14] M. Uchida, H.M. Kim, T. Kokubo, M. Nawa, T. Asano, K. Tanaka, T. Nakamura, Apatite-forming ability of a zirconia/alumina nanocomposite induced by chemical treatment, J. Biomed. Mater. Res. 60 (2002) 277–282.
[15] W. Wu, G.H. Nancollas, Interfacial free energies and crystallizations in aqueous media, J. Colloid Interface Sci. 182 (1996) 365–373.
[16] A.S.A. Chinellato, A.L. Chinellato, C.L. Ojaimi, J.A. Ferreira, E.M.J.A. Pallone, Effect of sintering curves on the microstructure of alumina-zirconia nanocomposites, Ceram. Int. 40 (2014) 14669–14676.
[17] A.S.A. Chinellato, E.M.J.A. Pallone, A.M.S. Souza, M.K. Manosso, A.L. Chinellato, R. Tomasi, Mechanisms of microstructure control in conventional sintering, in: A. Lakshmanan (Ed.)Sintering of ceramics-new emerging techniques, Intech, InTech Europe, Croatia, 2012, pp. 401–422.
[18] ASTM C1327–96, Standard Test Method for Vickers Indentation Hardness of Advanced Ceramics, Annual Book of ASTM Standards (2003).
[19] ASTM C-1421-99, Standard test method for determination of fracture toughness of

advanced ceramics, Annual Book of ASTM Standards (2001).
[20] P. Palmero, Structural ceramic nanocomposites: a review of properties and powders synthesis methods, Nanomaterials 5 (2015) 656–696.
[21] H. Bougherara, R. Zdero, A. Dubov, S. Shah, S. Khurshid, E.H.A. Schemitsch, Preliminary biomechanical study of a novel carbon-fibre hip implant versus standard metallic hip implants, Med. Eng. Phys. 33 (2011) 121–128.
[22] E. Nouri, M. Shahmiri, H. Reza Rezaie, F. Talayian, The effect of alumina content on the structural properties of ZrO_2-Al_2O_3 unstabilized composite nanopowders, Int. J. Ind. Chem. 3 (17) (2012) 1–8.
[23] A. Karthik, P. Manivasakan, S. Arunmetha, R. Yuvakkumar, V. Rajendran, Production of Al_2O_3-stabilized tetragonal ZrO_2 nanoparticles for thermal barrier coating, Int. J. Appl. Ceram. Technol. 10 (6) (2013) 887–899.
[24] R.N. Wenzel, Resistance of solid surfaces to wetting by water, Ind. Eng. Chem. 28 (1936) 988–994.
[25] M.L. Brandão, T.B.D. Esposti, E.D. Bisognin, N.D. Harari, G.M. Vidigal Jr, M.B. Conz, Surface of dental implants x biological response, Imp. News Mag. 7 (1) (2010) 95–101.
[26] P.G. Gennes, Wetting: statics and dynamics, Rev. Mod. Phys. 57 (1985) 827–863.
[27] L.L. Hench, Bioceramics, J. Am. Ceram. Soc. 81 (7) (1998) 1705–1728.
[28] M. Boix, S. Eslava, G. Costa Machado, E. Gosselin, N. Ni, E. Saiz, J. De Coninck, ATR-FTIR measurements of albumin and fibrinogen adsorption: inert versus calcium phosphate ceramics, J. Biomed. Mater. Res. Part A 103 (11) (2015) 3493–3502.
[29] Joint Committee For Powder Diffraction Studies (JCPDS), Diffraction Data Base, Newton Square: International for Diffraction Data (2003).
[30] D. Mcconnell, Apatite: its crystal chemistry, mineralogy, utilization, and geologic and biologic occurrences, Appl. Mineral. 5, Springer: Elsevier (2012).
[31] C. Rey, C. Combes, C. Drouet, S. Cazalbou, D. Grossin, F. Brouillet, S. Sarda, Surface properties of biomimetic nanocrystalline apatites; applications in biomaterials, Prog. Cryst. Growth Charact. Mater. 60 (3–4) (2014) 63–73.
[32] J.M. Hughes, J.F. Rakovan, Structurally robust, chemically diverse: apatite and apatite supergroup minerals, Elements 11 (2015) 165–170.
[33] S.V. Dorozhkin, Calcium orthophosphate deposits: preparation, properties and biomedical applications, Mater. Sci. Eng., C. 55 (2015) 272–326.
[34] A. Wennerberg, T. Albrektsson, R. Jimbo, Implant Surfaces and Their Biological and Clinical Impact, Springer, Berlin, Heidelberg, 2015.
[35] R. Trindade, T. Albrektsson, A. Wennerberg, Current concepts for the biological basis of dental: foreign body equilibrium and osseointegration dynamics implants, Oral. Maxillofac. Surg. Clin. North Am. 27 (2015) 175–183.
[36] S. Ramakrishna, M. Ramalingam, T.S.S. Kumar, W.O. Soboyejo, Biomaterials: A Nano Approach, CRC Press, 2016.
[37] B. Ben-Nissan, Advances in Calcium Phosphate Biomaterials, Springer, Berlin, 2014.
[38] I. Denry, L.T. Kuhn, Design and characterization of calcium phosphate ceramic scaffolds for bone tissue engineering, Dent. Mater. 32 (2016) 43–53.
[39] I. Antoniac, S. Cosmin, A. Antoniac, Adhesion aspects in biomaterials and medical devices, J. Adhes. Sci. Technol. 30 (16) (2016) 1711–1717.